AD-A068 663 BOLT BERANEK AND NEWMAN INC CAMBRIDGE MASS F/G 5/8
AUTOMATED PROCESSING OF SATELLITE IMAGERY DATA: TEST OF A SPECT--ETC(U)
MAR 79 R M PICKETT, E S BLACKMAN F19628-77-C-0164
UNCLASSIFIED BBN-4053 AFGL-TR-79-0040 NL

| OF |
AD
A068663

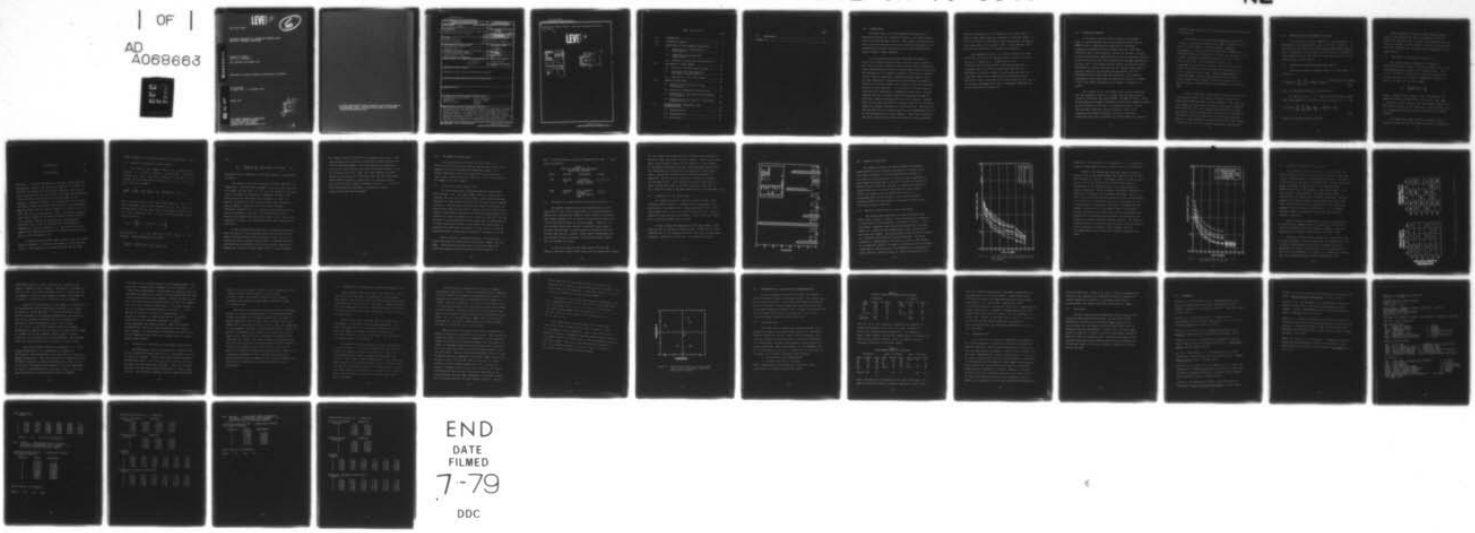

END
DATE
FILMED
7-79
DDC

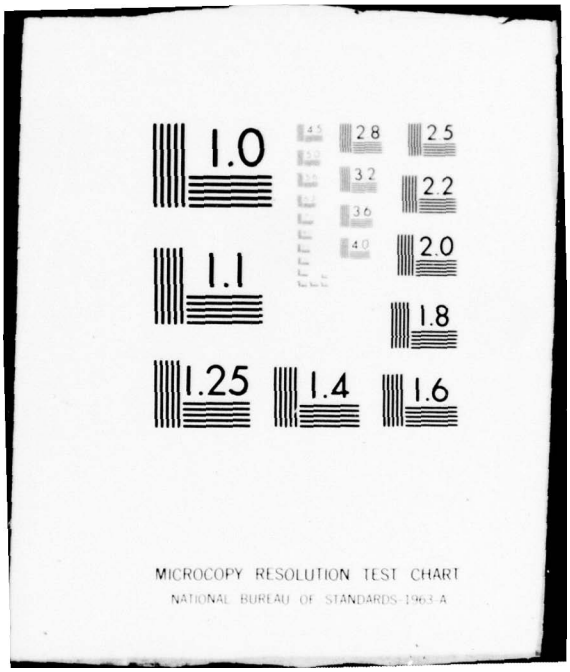
1.0
1.1
1.25
1.4
1.6
1.8
2.0
2.2
2.5
2.8
3.2
3.6
4.0
4.5
MICROCOPY RESOLUTION TEST CHART
NATIONAL BUREAU OF STANDARDS-1963-A

LEVEL II

(6)

B.S.

AFGL-TR-79-0040

AUTOMATED PROCESSING OF SATELLITE IMAGERY DATA: TEST OF A SPECTRAL CLASSIFIER

Ronald M. Pickett
Elliott S. Blackman

Bolt Beranek and Newman Inc.

Final Report
11 April 1977 - 31 January 1979

March 1979

AIR FORCE GEOPHYSICS LABORATORY
AIR FORCE SYSTEMS COMMAND
UNITED STATES AIR FORCE
HANSCOM AFB, MASSACHUSETTS 01731

UNCLASSIFIED

SECURITY CLASSIFICATION OF THIS PAGE (When Data Entered)

REPORT DOCUMENTATION PAGE		READ INSTRUCTIONS BEFORE COMPLETING FORM
1. REPORT NUMBER AFGL-TR-79-0040	2. GOVT ACCESSION NO.	3. RECIPIENT'S CATALOG NUMBER
4. TITLE (and Subtitle) Automated Processing of Satellite Imagery Data: Test of a Spectral Classifier		5. TYPE OF REPORT & PERIOD COVERED Final Report, 11 April 1977 — Jan 1979 6. PERFORMING ORG. REPORT NUMBER BBN Report 4053
7. AUTHOR(s) Ronald M. Pickett Elliot S. Blackman		8. CONTRACT OR GRANT NUMBER(s) F19628-77-C-0164
9. PERFORMING ORGANIZATION NAME AND ADDRESS Bolt Beranek and Newman Inc. 50 Moulton Street Cambridge, MA 02138		10. PROGRAM ELEMENT, PROJECT, TASK AREA & WORK UNIT NUMBERS 62101F 667008AD
11. CONTROLLING OFFICE NAME AND ADDRESS Air Force Geophysics Laboratory Hanscom AFB, MA 01731 Monitor/Thomas J. Keegan/LYU		12. REPORT DATE March 1979 13. NUMBER OF PAGES 43
14. MONITORING AGENCY NAME & ADDRESS(if different from Controlling Office)		15. SECURITY CLASS. (of this report) UNCLASSIFIED 15a. DECLASSIFICATION/DOWNGRADING SCHEDULE

16. DISTRIBUTION STATEMENT (of this Report)

Approved for public release; distribution unlimited.

17. DISTRIBUTION STATEMENT (of the abstract entered in Block 20, if different from Report)

18. SUPPLEMENTARY NOTES

19. KEY WORDS (Continue on reverse side if necessary and identify by block number)

automated picture processing
mephanalysis
spectral analysis
pattern recognition
satellite imagery
accuracy
scaling

20. ABSTRACT (Continue on reverse side if necessary and identify by block number)

This report details the development and testing of algorithms for automated classification of Very High Resolution (VHR) cloud imagery from orbiting weather satellites. The imagery data are first processed into average wave number spectra. The spectral features are then input to a Bayesian quadratic discriminant classifier. The classifier is designed to work with VHR visual and IR data, but was tested here on VHR visual data alone. Comparison of the classifier to a "blind" processor using a priori →

next page

DD FORM 1 JAN 73 1473 EDITION OF 1 NOV 65 IS OBSOLETE

UNCLASSIFIED 060 100

SECURITY CLASSIFICATION OF THIS PAGE (When Data Entered)

probabilities shows accuracy of classification appreciably better than chance.

LEVEL II

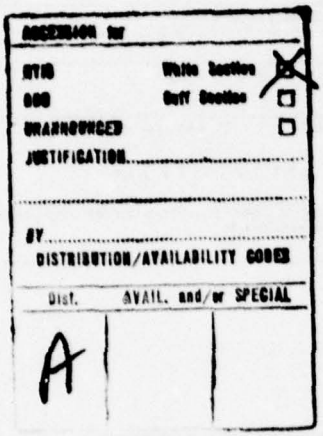

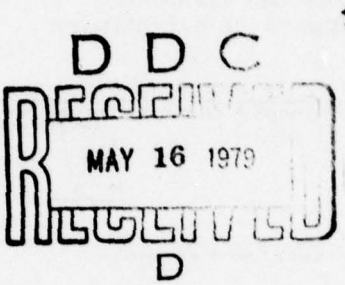

Table of Contents

Page

1.Ø INTRODUCTION

We report here on the development and testing of an automated technique for classifying clouds in the visual imagery from an orbiting weather satellite. This study is the core of an effort to select and test certain algorithms for eventual use in automated cloud imagery processing at Air Force Global Weather Central (AFGWC), Omaha, Nebraska.

In the program as originally conceived, we hoped to exploit the highest resolution data, fine mode at Ø.3 nautical mile (nm) per pixel, from both visual and IR sensors on board the Defense Meteorological Satellite Program (DMSP) Block 5D satellites. The approach was to be based on annularly integrated or averaged Fourier spectral amplitudes, termed wave number spectra, used as input features to a multivariate normal Bayesian classifier. Similar prior studies (Booth, 1973; Sikula, 1974) have indicated potential in the procedure. For a plethora of reasons ranging from satellite instability, to AFGWC work priorities, to McIDAS hardware failure, no Block 5D data were processed through the classifier, despite the best efforts of all involved. Although Block 5C data were processed as a backup, they did not include IR imagery at adequate resolution for classification. Resolution of the available IR was 6 times coarser than the approximately Ø.3 to Ø.7 nm resolution of the visual imagery. Thus, while conducting the cloud classification study with visual data alone provided

insight and experience in the operation of a cloud classifier based on wave number spectral components as features, absence of the richer source of information from the data base (IR imagery, as witness Booth, 1973; Koffler, 1973; Lo and Johnson, 1971), was a serious limitation to classifier performance.

The subsequent body of this report consists of a brief historical overview of the present project and prior work that led up to it (Section 2); a description of the automated classifier that was tested here, including the specific signal processing and classification algorithms (Section 3); a description of the test sample of cloud images and the associated truth data (Section 4); presentation of the study results (Section 5); and a discussion of the significance of our findings for further development and study of automated techniques for cloud classification (Section 6).

2.0 HISTORICAL OVERVIEW

In an earlier contract effort (Pickett and Blackman, 1976), it was determined that the most promising next step for AFGWC to take in upgrading its capability for automated processing of weather satellite imagery data was to develop a classifier that utilizes spectral features of the data. As part of that initial effort, demonstrations of Fourier spectral analysis of three cloud types were also conducted and reviewed (Blackman and Pickett, 1977). The present project carried the process forward. Algorithms for spectral analysis and for classification based on spectral features, were selected and programmed, with most programming done by AFGL under BBN direction. The classifier comprised of these algorithms was empirically tested on a sample of 158 cloud images representing six different categories of clouds.

The original aim of the present effort was to develop and test the automated classifier on images from the most advanced series of satellites now serving AFGWC, the DMSP 5D series. These 5D satellites can transmit coincident IR and visual imagery at nomi al spatial resulution of Ø.3 nm. Our objectives were to see not only how good a spectral feature classifier might be for effective and efficient digestion of data at that high a resolution, but also to determine the effectiveness of a spectral

classifier using visual alone, IR data alone and IR and visual data in combination.

The plan was to do initial development and testing of the classifier on available imagery from a DMSP 5C satellite, but to switch to 5D data when it became available. Repeated postponements of the delivery of 5D data led to adoption of contingency plans for debugging and testing the classifier on the 5C data. Plans for eventually using the 5D data were several times revised, but it was necessary finally to abo. altoqether for utilizing the 5D data, and the contract effo. eventually focused entirely on testing and analyzing performance of the classifier with 5C data. Because simultaneous 5C I visual VHR images at equal resolutions are not available, t primary impact of this change in plans with respect to the st goals was that it limited testing the classifier to just visual data.

To ensure continuity of the present effort with continuing related work at AFGL, the contract called for coding of the algorithms by AFGL personnel on AFGL computers. Also, the truth data, based on visual classifications of the imagery samples as described below, had to be accomplished by personnel at AFGL. The success of this overall effort in spite of the difficulties encountered is due in no small part to the highly responsive behavior of AFGL personnel in adjusting and timing their support in these areas to suit the changing study plans and schedule.

3.0 DESCRIPTION OF THE AUTOMATED CLASSIFIER

Our description of the classifier is in three parts: 1) processing of the raw satellite data into power spectra; 2) conversion of the power spectra into average wave number spectra; and 3) computation of the classification statistics. We discuss each step briefly here and refer the reader to section 3.2 of our earlier report for more detail.

3.1 Computation of Two-Dimensional Power Spectra

The Discrete Fourier Transform (DFT) in two dimensions is defined as

$$\hat{a}(f_x, f_y) = \sum_{j=1}^{N} \sum_{k=1}^{M} a[j(\Delta x), k(\Delta y)]\, e^{-i2\pi [jf_x(\Delta x) + kf_y(\Delta y)]} \tag{1}$$

with $\hat{a} \leftrightarrow a$ representing Fourier transform pairs.

If we let $N = M$, $\Delta x = \Delta y = T/N$ (with T the analysis window size), and compute f_x, f_y only at integer multiples of T^{-1}, then

$$\hat{a}(n,m) = \sum_{j=1}^{N} \sum_{k=1}^{N} a\left(\frac{jT}{N}, \frac{kT}{N}\right) e^{\frac{-i2\pi}{N}(jn + km)} \tag{2}$$

which is a defining form for the FFT.

Computing Equation 2 using the FFT algorithm produces an array of data representing the first quadrant in the two dimensional spectral plane. Because of the spectrally periodic nature of the FFT, the entire spectral plane can be generated from first quadrant data, allowing direct computation of wave number spectra.

3.2 Computation of Average Wave Number Spectra

Wave number spectral components are computed as spectral amplitudes ($\hat{a}(n,m)$) for those elements falling within corresponding annular bands in the frequency plane. Each band is one unit in width and symmetrically disposed radially about integer multiples of the radial "fundamental" frequency 1/T. That is, at least for n,m <N/2, compute

$$p = \left[\sqrt{n^2 + m^2} + .5 \right] \qquad (3)$$

where [ ] extracts the greatest integer not exceeding the expression within, and add $\hat{a}(n,m)$ to the pth wave number. It is important to note, however, that wave numbers computed from FFT indices directly are not referenced to the principal part of the (aliased) spectrum when either index exceeds the Nyquist frequency.

To compute wave number spectra as sums over annular regions, we subtract any given index from N if it exceeds N/2:

$$n' = \min(n, N-1) \tag{4}$$

$$m' = \min(m, N-m) \tag{5}$$

where min( ) extracts the smaller of the two values within the parentheses. Equation (3) may then be applied to n' and m' to determine the proper total wave number spectrum. Here, we are merely exploiting the periodic nature of the FFT and representing n and m by their values within the principal part of the spectrum. Although we require this shifted data to fall within the Nyquist region or principal spectral part, this requirement does not simply limit the useful range of p to $p \leq N/2$, since it is clear that $f_x = f_y = N/2$ yields $p = \frac{\sqrt{2}}{2} N$. In essence, aliasing occurs above frequencies given by the square region constraint ($|f_x|, |f_y| \leq N/2$) and not by any equivalent one-dimensional constraint on p. Thus, we ultimately use the NxN spectral components of the first quadrant, i.e., all the FFT data, but combine their magnitudes based on first applying Equations (4) and (5), and then Equation (3).

To generate average wave number spectra, each wave number spectral component is divided by the number of terms that went into it. The components are scaled such that the zero wave

number component is the average value of the spatial data array.

3.3 Quadratic Discriminant Classification

The average wave number spectra are treated as input features to a Bayesian quadratic discriminant classifier. Treating the class conditional probability densities for the feature vectors as multivariate normal, we have (see Duda and Hart, 1973, for example)

$$g_i(\underline{a}) = -\frac{1}{2}(\underline{a} - \underline{\mu}_i)^t \Sigma_i^{-1}(\underline{a} - \underline{\mu}_i) - \frac{1}{2}\log|\Sigma_i| + \log P(c_i) \qquad (6)$$

Here, $\underline{a}$ is the feature vector (wave number spectra), "t" denotes matrix transpose, $g_i(\underline{a})$ the discriminant for the ith class, $\underline{\mu}_i$ the mean vector for that class, $P(c_i)$ the *a priori* probability of ith class occurrence, and Σ_i the ith covariance matrix with elements given by

$$\sigma_{jk/i} = E\left[(a_{j/i} - \mu_{j/i})(a_{k/i} - \mu_{k/i})\right] \qquad (7)$$

The operator $E\{\quad\}$ is the expectation with respect to the ensemble. Expanding Equation (6) yields

$$g_i(\underline{a}) = -\frac{1}{2}\,\underline{a}^t\,\Sigma_i^{-1}\,\underline{a} + (\Sigma_i^{-1}\,\mu_i)^t\underline{a} + \theta_i \qquad (8)$$

with

$$\theta_i = -\frac{1}{2}\,\underline{\mu}_i^t\,\Sigma_i^{-1}\,\underline{\mu}_i - \frac{1}{2}\log|\Sigma_i| + \log P(c_i) \qquad (9)$$

The general form of Equation (8) indicates quadratic discriminant functions.

Our concern is for the efficiency and hence simplicity of computation. Since we need to compute θ_i once for each class and can compute once and store $(\Sigma_i^{-1}\,\underline{u}_i)^t$ as a new vector $\underline{u}'_i$ for each class, the potential computational complexity resides in the first term on the right hand side of Equation 8. While in general, an NxN matrix will require N^2+N multiplications and a similar number of additions (for each class), we make a reasonable assumption Σ_i^{-1} is a diagonal matrix and thus we can scale each element of $\underline{a}$ by its class conditional standard deviation and compute the norm of the scaled vector. This latter computation requires only 2N multiplications and N additions for each class.

In the classification experiment as conducted with visual data from Block 5C, the covariance matrix was estimated by the sample covariance matrix, with off-diagonal terms set to zero. Had we been able to process Block 5D data, a somewhat different covariance matrix estimator would have been used, comprising 4 submatrices, each with nonzero terms only on its main diagonal.

The composite matrix would be of tri-diagonal form, with nonzero terms wherever the correlation coefficient involves two elements with the same wave number. Also considered was an additional feature for classification, the cross-correlation between visual and IR data at zero lag. Thus, for N wave numbers, the basic feature vector would be of size 2N+1, with the covariance matrix having $(2N+1)^2$ elements, of which 4N+1 are nominally nonzero. Because of the large number of elements involved (N was 53 in the video classification experiment), coalescence of wave spectra would have been performed.

4.0 THE SAMPLE OF CLOUD IMAGES

This description is divided into three parts: 1) Specification of the satellite and of the particular orbits and segments of orbits from which the images were taken; 2) a general description of the test images and the procedures for their visual classification and selection; and 3) an overview of the composition of the sample.

4.1 Satellite and Orbit Specification

The cloud images were recorded by DMSP 5C vehicle 5528 during August, 1972. The image samples that were analyzed were selected from very high resolution (VHR) visual records that were displayed on a Man-Computer Interactive Data Access System (MCIDAS) TV screen. Infrared high resolution (HR) images of the same area taken at the same time were used to assist in cloud classification. Details of the spatial resolution of the visual and IR sensors on 5C vehicles are given in Nichols, et al. (1975, pp. 186-187). For the central 2/3 of the satellite's cross-track scan, to which selection of visual images was limited in this study, the nominal spatial resolution for VHR visual is between 1/3 and 3/4 nm. For the HR infrared imagery, corresponding resolution is between 2 and 4 nm.

Vehicle 5528 was a noontime satellite. The particular orbits from which the images were selected were numbers 5790 and 6200. Selection was from that part of each orbit where the vehicle was passing over the vicinity of Central America.

Table 1 gives the general location, background and range of cloud types encountered.

TABLE 1
ORBITS OF VEHICLE 5528 FROM WHICH IMAGES WERE SELECTED

ORBIT	LATITUDE	BACKGROUND	CLOUDS
5790	NORTHERN LOW	CARIBBEAN CENTRAL AMERICA EASTERN PACIFIC	Ci, Cb, Cu, Cs
6200	NORTHERN LOW	GULF OF MEXICO CARIBBEAN FLORIDA, MEXICO, CUBA	Ci, Cb, Ac, Sc

4.2 Procedures for Image Selection and Visual Classification

The general approach was to have meteorologists, highly experienced in the visual interpretation of satellite images, examine full resolution TV images to find, classify, and excerpt small square regions (75 x 75 pixels) of the pictures containing single cloud types, to serve as the test images. Mixes of clouds such as might occur where regions of different cloud types at the same altitude meet, or where clouds at different altitudes overlap, were strictly avoided. Mixed (shore) backgrounds were also avoided as much as possible, and excerpted sample images were not allowed to overlap.

In the first stage of the visual search for the test images, large scale views of both visual and IR imagery were examined.

For this stage, the visual data were electronically degraded to match the lower resolution if the IR imagery. These paired large-scale views provided a basis for the observer to orient himself to the general geographic location, the background against which the clouds had to be interpreted and recognized (land, water, shore), and general features of the cloud distribution at mesoscale. The IR data were important in helping to separate low and high clouds. Final distinctions among cloud types at a given altitude were made on the basis of visual inspection of full resolution views of the VHR visual data for each candidate image.

4.3 Composition of the Image Sample

An attempt was made to find test images in each of the following eight categories: cumulus (Cu), stratocumulus (Sc), stratus (St), altocumulus (At), altostratus/nimbostratus (As/Ns), cumulonimbus (Cb), cirrus (Ci), and cirrostratus (Cs). Several samples of clear sky were also sought. In all, 158 cloud images and 14 clear-sky samples were selected.

Figure 1 shows the composition of the image sample. Most numerous (66) are images of cumulus clouds. Middle-level clouds (As/Ns and Ac) all by themselves did not occur with any appreciable frequency. No As/Ns or St and just 2 Ac samples were found.

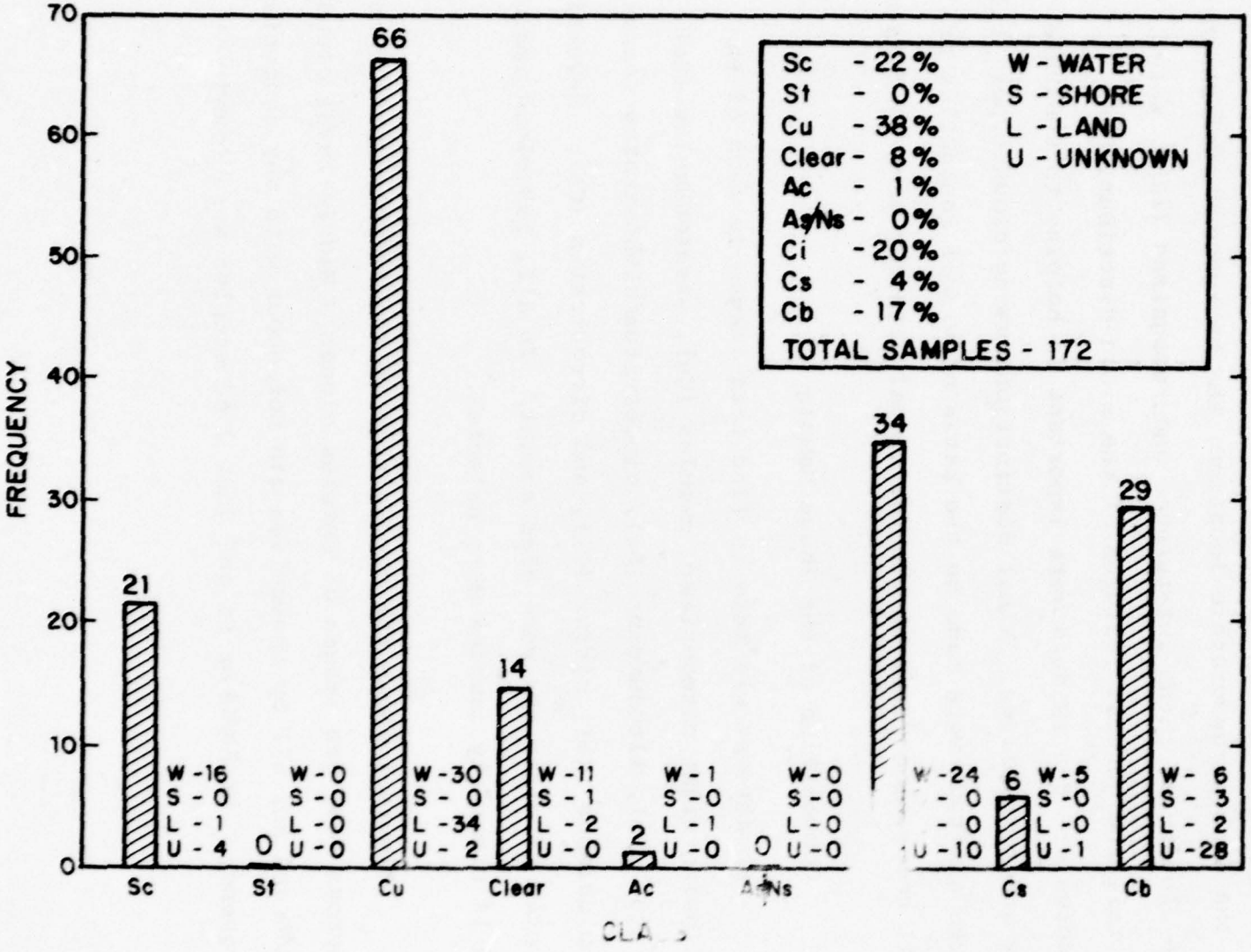

Figure 1. Frequencies of cloud types and backgrounds in the test sample.

5.Ø RESULTS OF THE STUDY

We present first what we found regarding the spectral characteristics of the various cloud types as a result of just the signal processing. We then examine the performance of the classifier, how accurately it classifies, what confusions it makes among the clouds when it does err, and how that pattern of confusions may be taken into account in estimating accuracy of classification were the cloud types optimally partitioned. Finally, we report on the procedure and results of a multidimensional scaling analysis of the error data which provides insight into the number of orthogonal dimensions used effectively by the classifier.

5.1 Spectral Characteristics of the Cloud Types

The average wave amplitudes for each of the six cloud types found is given in Figure 2. The discriminating information in this family of curves appears to be mainly in the d.c. (zero wave number) components and in one or two properties of overall shape, e.g., bandwidth and/or amplitude at some representative mid range wave number. Not surprisingly, Cb has by far the largest d.c. component and Cu has the greatest bandwidth. The clear category is, appropriately, the lowest in both of these aspects. It is important, however, to temper interpretation of the apparent orderliness of these data with a consideration of variability of these functions, smooth as they are, among realizations within

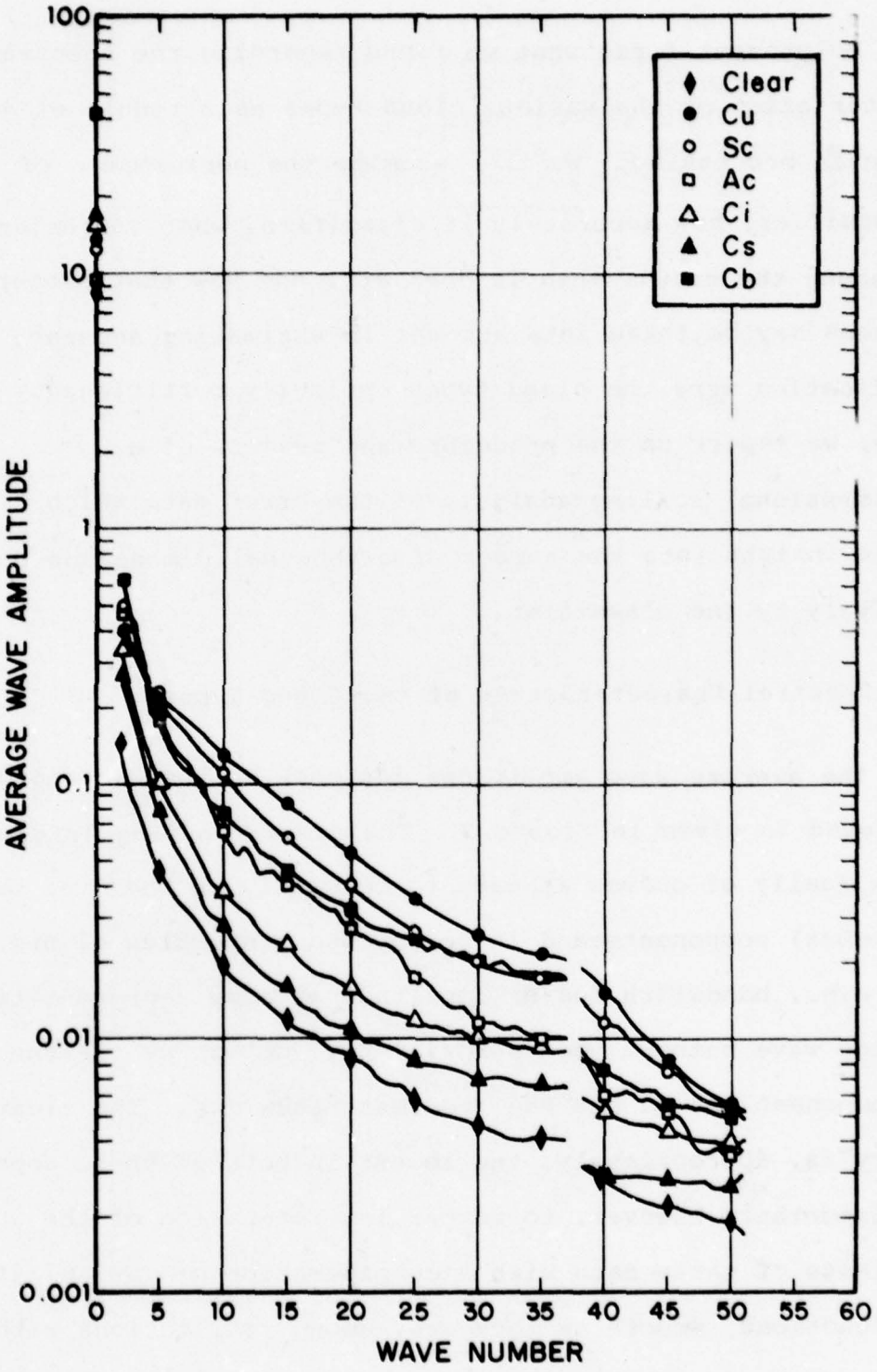

Figure 2. Wave amplitude spectra averaged over all realizations for each cloud type in the test sample.

categories. The variability is substantial, as is illustrated in Figure 3, which shows the six realizations for the Cs category.

Breaks in the average wave amplitude spectral plots of Figures 2 and 3, occurring between wave numbers 37 and 38, have been inserted for clarity. The abrupt change in level for many but not all of the curves as they transit this region, is believed due to the combined effects of aliasing and minor pattern anisotropy. As stated above, the Nyquist frequency is a function of orientation for two-dimensional FFTs. Here, it is $75/2 = 37.5$ in vertical and horizontal directions, and increases to $75/\sqrt{2} \simeq 53$ at $\pi/4$ multiples that are not multiples of $\pi/2$. If a cloud pattern is anisotropic such that its spectrum extends further in the vertical or horizontal than at any diagonal azimuth, aliasing will be more severe than if the pattern were aligned with its maximum spectral extent coincident with the direction of minimal aliasing (maximal Nyquist). The impact of anisotropy and its interaction with aliasing on the performance of the classifier is unknown. Note, however, that the semi-logarithmic nature of the plots greatly exaggerates the effect.

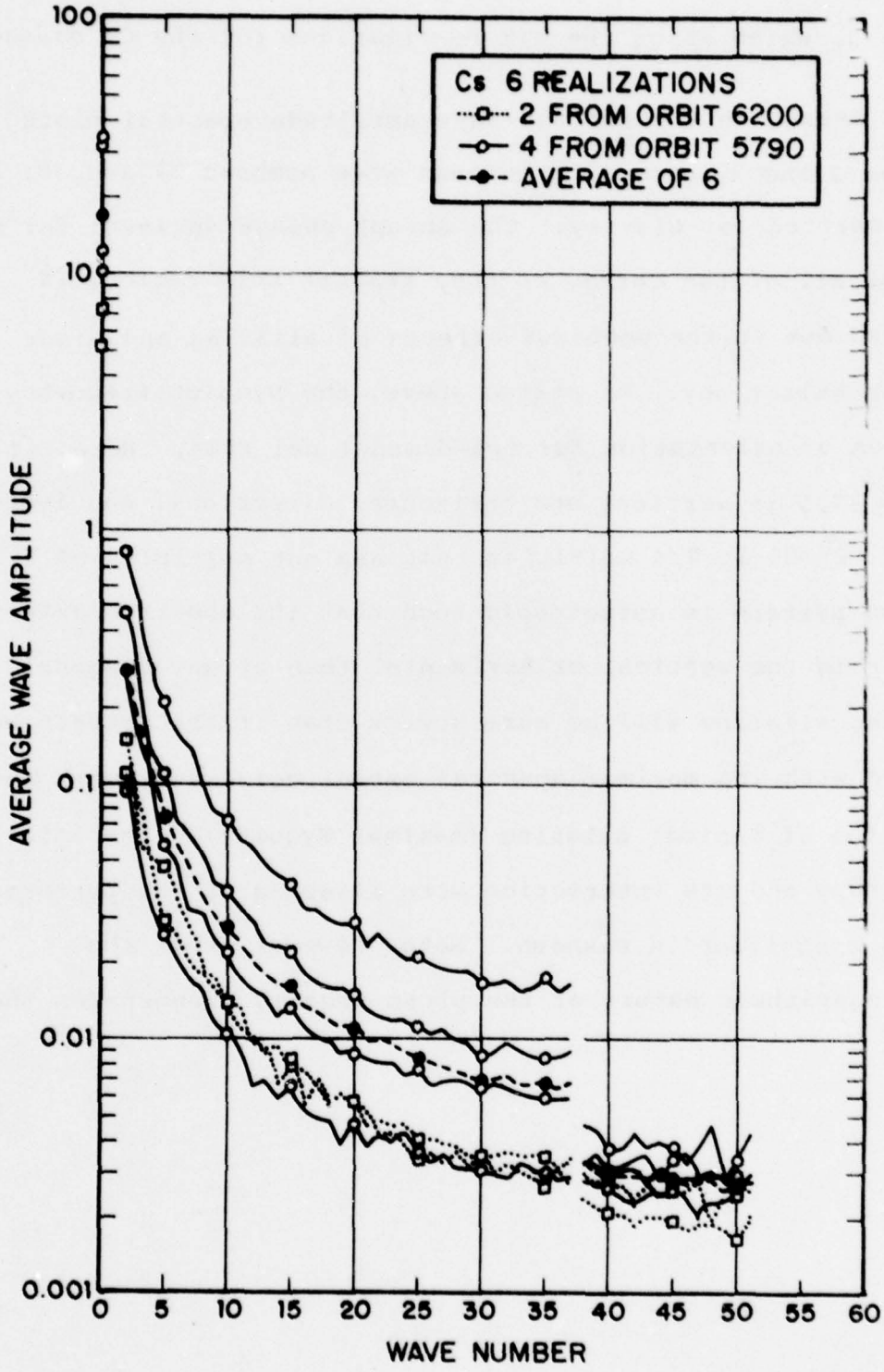

Figure 3. Wave amplitude spectra for the six realizations of Cs clouds.

5.2 Accuracy of Automated Classification

The accuracy of classification is derived from the data given in Figure 4 in the form of two matrices, which relate true (visual) classification to automated classification. The matrix on the left gives the data in frequency form. On the right they appear in probability form, which is the frequency form normalized to unity. The columns of each matrix stand for the true (visual) classifications. The rows stand for the classification as issued by the automated classifier. The main diagonal cells (those running from the upper left to the lower right corner) show in the left (right) matrix the frequencies (probabilities) of correct classification, i.e., the number (relative number) of samples of each cloud type that were correctly classified.

Overall accuracy (probability of correct classification) is determined by summing over the frequencies in the diagonal cells and dividing by the total number of samples. Thus the probability of a correct classification is 72/158 = 0.46.

Accuracy of classification within each of the cloud types is also of interest. The cloud type with the highest probability of correct classification is Cs, with a probability of 0.83. Probability of correct classification is no less than 0.38 for any of the six categories. Of course, it is important to observe that the confidence bounds for these probabilities vary

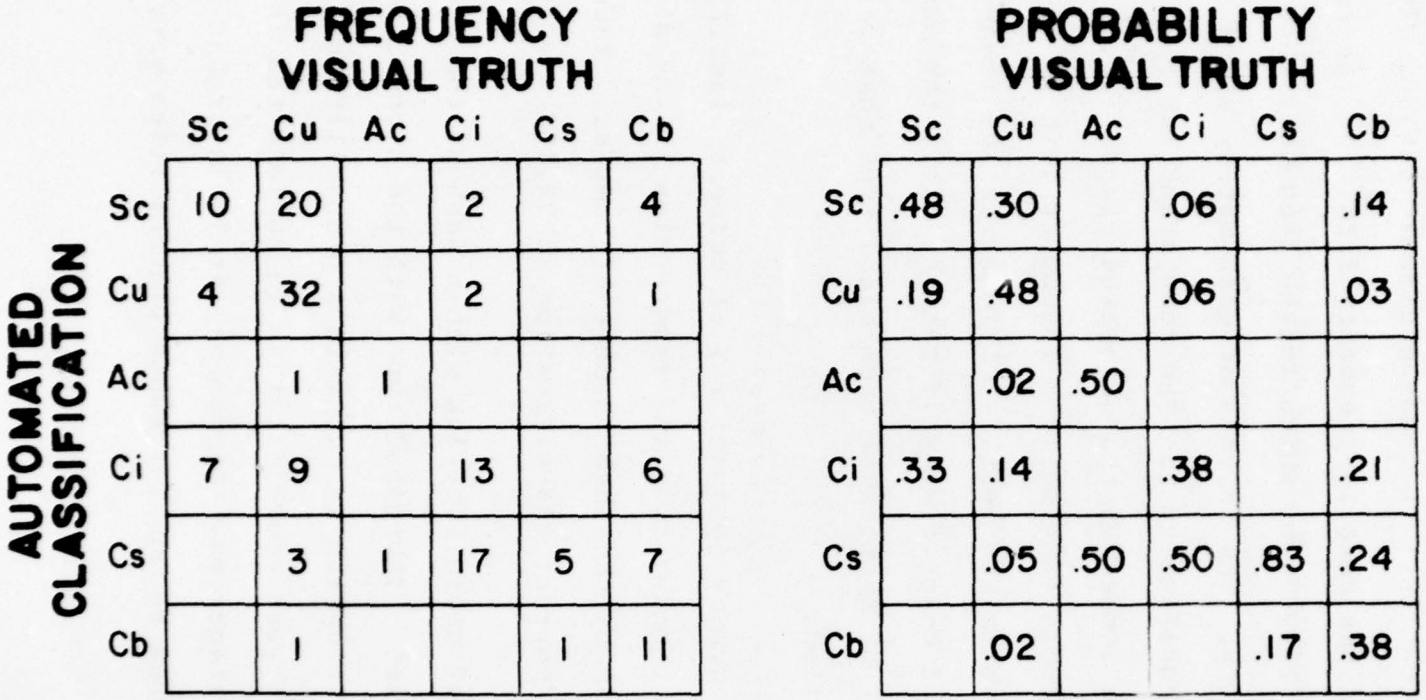

Figure 4. Matrices showing accuracy of classifica , frequency data on the left and probability data on the ht.

considerably from one class to another as a function of the number of samples in each category. Performance in category Ac, where p = Ø.5, is not well estimated, since it is based on only two samples. A similar small sample disclaimer can be made for Cs, where p = Ø.83, since it is based on only six samples.

Accuracy of classification on the sample as a whole has to be gauged against chance performance following one or another strategy by a "blind observer". If the blind observer works without knowledge of the a priori probabilities, and knows only what the six possible categories are, all strategies are equivalent. Chance performance yields on the average p = 1/6 = Ø.17. If the blind observer knows the a priori probabilities, then the best strategy is to classify every sample as a member of the most probable category, which, in this situation, is Cu with 66 out of the 158 samples. That strategy would allow the blind observer to attain p = 66/158 = Ø.42.

Since the automated classifier is Bayesian, i.e., uses a priori probabilities, it is appropriate to compare its performance to the performance of the blind observer using the a priori probabilities. Thus, the unconditional comparison of the automated classifier to chance classification is Ø.46 to Ø.42. On the face, the classifier performance is not very impressive, but there is considerably more to be said. First, it is clear from the pattern of classifications, that the automatic

classifier is not leaning heavily on the a priori probabilities. Note that it assigns only 39 samples to the Cu category. Also, of particular significance is the pattern of confusions when the automated classifier errs, and how its performance improves when certain cloud categories are combined. Finally, we must consider the class conditional performance taken as a whole and compared with the class conditional performance of the blind observer. For Cu, of course, the blind observer is perfectly accurate, whereas for any other class, he is always wrong. In c except for Cs which is a small class with 6 occurrences, performance of the automated classifier is closely class-independent as regards accuracy. While the accuracy of the automated visual classifier leaves something to be desired (TR data, perhaps), its performance is consistent with the 1,Ø cost function implicitly used (all errors equally bad, all correct answers equally good).

5.3 Information in the Pattern of Confusions: Partitioning

The off-diagonal cells in the matrices of Figure 4 show how the classifier performs when it errs. The pattern of errors is clearly not random. Certain cloud types are more probably confused than others. Note that the errors tend to cluster in the upper left and lower right quadrants. Thus, for the super categories (ScCuAc Versus CiCsCb), performance is rather highly accurate. The automated classifier calls a sample from ScCuAc

either Sc, Cu, or Ac with p = 68/89 = Ø.74. Similarly, it calls a sample from the CiCsCb either Ci, Cs or Cb with p = 61/69 = Ø.88. The overall accuracy of the automated classifier with respect to these super categories is thus, p = 129/158 = Ø.82.

This level of accuracy, of course, also has to be gauged relative to chance, the performance of a blind observer which assigns every sample to the super category with the larger a priori probability, which in this case is ScCuAc, with its 89 samples out of the total of 158 (p = Ø.56). Thus, the comparison of the automated classifier to chance classification, taking the pattern of confusions into account in this particular way, is Ø.82 to Ø.56. Now we can see a substantial advantage of the classifier over chance. Of course, we have to acknowledge that this particular pattern of confusions would itself be subject to variation over repeated tests, and the exact nature of the pattern of confusions and how best to partition the sample so as to optimize performance of the classifier would depend on obtaining more reliable estimates of the confusion probabilities. We can only illustrate here the possible gains from such optimization.

5.4 Information in the Pattern of Confusions: Dimensionality

The automated classifier locates each sample in 53-space, each dimension of the space corresponding to a wave number. Hyperquadrics partition the space into mutually exclusive regions corresponding to each of the six cloud types. Samples, which by their wave amplitudes fall into a particular region of the space are classified as the cloud type corresponding to the region into which they fall.

While the classifier actually works in 53-space, we can ask whether it effectively uses that many dimensions. One way to answer that question is to see how many dimensions of variation among the samples are needed to account for the way the classifier confuses the various cloud types. We turn again to the confusion matrices in Figure 4.

Our approach to determining the effective dimensionality of the classifier is to treat the probabilities of confusion between cloud types as measures of similarity. Thus, we see from the probability matrix when Cu samples are presented, the classifier calls them Sc with probability 0.3. This relatively high probability of confusion between Cu and Sc we take to mean that they are seen by the classifier as highly similar. On the other hand, when Cu is presented it is almost never called Cb and we conclude that Cu and Cb are seen by the classifier as highly dissimilar.

These measures of similarity are input to a computer program [see Takane et al. (1977) and specifications in Appendix A of this report]) for nonmetric multidimensional scaling. That program treats these inputs as measures of the distance, in n-space, among the categories. It finds, for selectable values of n, that positioning of the six categories which best accounts for the distances in terms of similarity, and it measures how much of the variance of these distances is accounted for by the model. For n = 6, by definition, 100% of the variance can be accounted for. Is there a dimensionality less than 6 which accounts for essentially all of the variance?

What we find in this case is that only 3 dimensions are needed to account for over 98% of the variance. Thus, though the classifier nominally utilizes 53 dimensions in classifying the stimuli, the pattern of confusions suggests that the effective number of orthogonal dimensions being utilized (not necessarily one to one with any of the original wave number inputs) is no more than three. Each of those three dimensions could of course be derived from some combination of the wave number inputs, and we have no way of telling what those derivations are without conducting further studies beyond the scope of the present contract. However, we can look to see if there is any obvious relationship between any one of the three dimensions in the confusion model and observable dimensions of differences among the six average spectral functions shown in Figure 2. We have

already observed that they tend to differ in terms of the d.c. component and in terms of a few general features of shape related to mid range level or bandwidth. Could these features correspond to any of the dimensions in the confusion model?

From Figure 2 we see that with respect to magnitude of the d.c. component (height at wave number Ø) the cloud types order from low to high: Ac, Sc, Cu, Ci, Cs and Cb. Taking height of the curves at wave number 35 as our point of reference, we find that the order of cloud categories from low to high is: Cs, Ac, Sc, Cb, and Cu.

Our inspection of the positioning of the cloud types in the confusion model showed that the order of stimuli in dimension 1 of the model is almost identical to their order with respect to magnitude of the d.c. component; and that their order on dimension 3 is almost identical to their order at the representative high mid range wave number. The plot of the cloud types on dimensions 1 and 3 of the confusion model is given in Figure 5, and the reader can satisfy himself regarding these assertions.

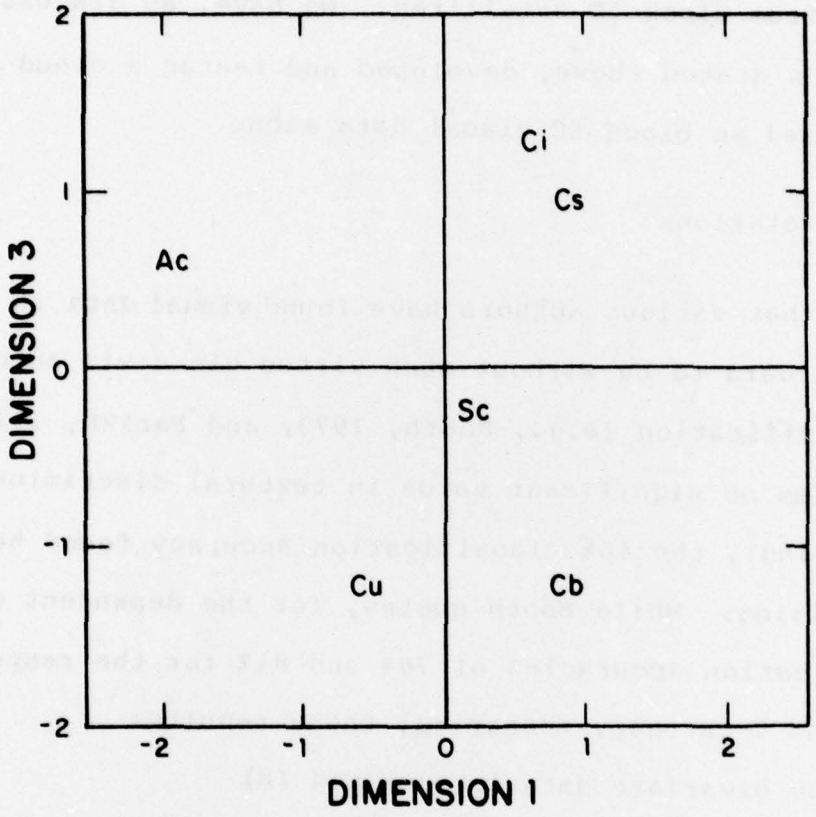

Figure 5. Plot showing locations of each cloud type in two of the three dimensions of the scaling model.

6.0 INTERPRETATIONS, CONCLUSIONS AND RECOMMENDATIONS

In this concluding section of the report, we attempt to place the present study in its proper context. The original aim was to develop and test a cloud classifier based on wave number spectra as features, jointly exploiting visual and IR fine mode data "saves" from Block 5D satellites. We have, as discussed and for the reasons stated above, developed and tested a cloud classifier based on block 5C visual data alone.

6.1 Interpretations

Given that various authors have found visual data in the absence of IR data to be without much virtue vis a vis automated Bayesian classification (e.g., Booth, 1973; and Parikh, 1977, 1978 who claims no significant value in textural discriminators for cloud typing), the 46% classification accuracy found here is hardly surprising. While Booth quotes, for the dependent data set, classification accuracies of 76% and 81% for the respective 6-category and 5-category scenarios, these results:

1) use bivariate data (visual and IR)

2) include clear sky as a category.

Table 2 shows the results from Booth's classifier, when classification is based on visual data alone.

TABLE 2
BOOTH'S CLASSIFIER BASED ON VISUAL ALONE

6-Category			5-Category		
Type	# cases	% correct	Type	# cases	% correct
Clear	113	75	Clear	113	65
Cu	258	60	Cu/Sc	413	59
Sc	155	35			
Cb	117	63	Cb	117	65
Ci	174	55	Ci	174	46
Ci+low	233	46	Ci+low	233	38
Totals:	1050	54		1050	54
No Clear:	937	52		937	52

Note that the 6- and 5-category classifiers each operates at roughly 54% accuracy, or at 52% if the clear category is artificially expunged from consideration. For comparison, Table 3 shows results from the wave number spectral classifier we have utilized, with 6-category, quasi 5-category, and quasi 4-category variations on the basic theme.

TABLE 3
WAVE NUMBER SPECTRAL CLASSIFIER

6-Category			Quasi 5-Category			Quasi 4-Category		
Type	#cases	%cor.	Type	#cases	%cor.	Type	#cases	%cor.
Sc	21	48	Sc	21	48	Sc/Cu	87	76
Cu	66	48	Cu	66	48			
Ac	2	50	Ac	2	50	Ac	2	50
Ci	34	38	Ci	34	38	Ci	34	38
Cb	29	38	Cb/Cs	35	69	Cb/Cs	35	69
Cs	6	83						
Totals:	158	46		158	51		158	66

Here, note that our 6 categories are all pure cloud types. The quasi-5 classifier refers to formally combining Cs and Cb into

one class, thereby representing a realizable though subop imal approximation to a 5-category system. Comparing the quasi-classifier to Booth's "6-category-minus-clear" results shows close parity, i.e., 51% to 52%. Combining Cu and Sc classifications produces the quasi-4 classifier. Comparing these results (66% correct) to Booth's 5-category-minus-clear (52% correct) shows the visual wave number spectral classifier in a better light. Taking all the above factors and comparisons into account, we view the present experiment as being con.. prior results and with our reasonable expectations, given the lack of IR data.

6.2 Recommendations

It is difficult to avoid the temptation to recommend that the original question of bispectral classifier performance be answered, when Block 5D data and the facilities to process the data are simultaneously available. Recent studies (Parikh, 1977 and 1978), suggesting that textural features are of little value for cloud classification, are not highly relevant to the success of classifying Block 5D imagery via wave number spectra because these studies used low resolution data and did not use wave number spectral components as textural features. Certainly, Parikh's classifier accuracies using only first order visual and IR statistical measures as features are impressive, but the number of cloud classes (3 or 4) and the class definitions were

not overly ambitious. There is an irony in Parikh's findings that texture is not important for automated classifiers, despite the central importance of texture to the weather expert who is providing the truth against which the classifiers are judged.

6.3 Conclusions

One small and preliminary experiment does not motivate the drawing of many profound conclusions. We have found strong morphological similarities in the wave number spectra of all cloud classes, but also quantitative differences sufficient for moderate classifier performance. Clearly, use of IR wave number spectra is expected to improve classifier performance, perhaps by some 20 to 30% as in Booth's study. The potential impact of the IR-visual cross correlation feature cannot easily be assessed, as we have been unable to find prior studies in which this obvious feature was used.

7.0 REFERENCES

Blackman, E. S. and Pickett, R. M., "Automated Processing of Satellite Imagery Data at Air Force Global Weather Central (AFGWC): Demonstration of Spectral Analysis," AFGL-TR-77-0080, 28 pages (1977).

Booth, A. L., "Cloud Type Pattern Recognition Using Environmental Satellite Data," Proc. First Intn. Joint Conf. Pattern Recognition, pp. 526-533 (1973).

Duda, R. O., and Hart, P. E., Pattern Classification and Scene Analysis, John Wiley and Sons, New York, 482 pages, (1973).

Koffler, R., et al., "A Procedure for Estimating Cloud Amount and Height from Satellite Infrared Radiation Data," Monthly Weather Review, 101(3); 240-243 (1973).

Lo, R. C., and Johnson, D. R., "An Investigation of Cloud Distribution from Satellite Infrared Radiation Data," Monthly Weather Review, 99(8): 599-605 (1971).

Nichols, D. A., Elsby, C. N., and Schultz, E. G., "Block 5D - Compilation," Defense Meteorological Satellite Program, Space and Missile Systems Organization, Air Force Systems Command, United States Air Force, 522 pages (1975).

Parikh, J., "A Comparative Study of Cloud Classification Techniques," Remote Sensing of Environment, 6, 67-81 (1977).

Parikh, J., "Cloud Classification from Visible and Infrared SMS-1 Data," Remote Sensing of Environment, 7, 85-92 (1978).

Pickett, R. M., and Blackman, E. S., "Automated Processing of Satellite Imagery Data at Air Force Global Weather Central (AFGWC): Survey, Recommendations and R & D Design Evaluation Report," BBN Report No. 3275 (1976).

Sikula, G. J., "Spectral Signatures of Several Cloud Types and Information Extraction from Very High Resolution Visual Satellite Radiances - Preliminary Results," Paper for Sixth Conference Aerospace and Aeronautical Meteorology, El Paso, Texas, 14 pages (November 12-14, 1974).

Takane, Y., Young, F. W., and deLeuw, J., "Nonmetric Individual Differences Multidimensional Scaling: An Alternating Least Squares Method with Optimal Scaling Features," Psychometrica, 42, 7-67 (1977).

```
ALSCAL (3) - DYNAMIC CORE ALLOCATION
V E R S I O N  (3.Ø1)

ALTERNATING LEAST SQUARES SCALING
AUGUST   1974
FINAL CHANGE 12/14/77

YOSHIO TAKANE , FORREST W. YOUNG & ROSTYSLAW J. LEWYCKYJ.
PSYCHOMETRIC LABORATORY
THE UNIVERSITY OF NORTH CAROLINA
CHAPEL HILL, N.C.  27514

COPYRIGHT 1977 FORREST W. YOUNG, YOSHIO TAKANE & ROSTYSLAW J. LEWYJKYJ

JOB TITLE: CLOUD CONFUSIONS

DATA SPECIFICATIONS-
 NB    - NUMBER OF STIMULI                  6   STIMULI
 NS    - NUMBER OF SUBJECTS                 1   SUBJECTS
 NDTYP- MEASUREMENT LEVEL                   3 = ORDINAL
 NSIM  - DATA TYPE                          3 = ASYMMETRIC-SIMILARITY
 NPS   - MEASUREMENT PROCESS                1 = DISCRETE
 NWC   - MEASUREMENT CONDITIONALITY         1 = SUBJECT CONDITIONAL
 NDMX  - NUMBER OF CELLS FOR TIES           36   CELLS

ANALYSIS SPECIFICATIONS-

 NWE   - MODEL TYPE                2 = ASYMMETRIC EUCLIDIAN (ASYMSCAL)
 NDIM  - NO OF DIMENSIONS (MAX)    3   DIMENSIONS (MAX)
 NDMN  - NO OF DIMENSIONS (MIN)    2   DIMENSIONS (MIN)
 NNC   - NEG WEIGHTS PERMITTED     Ø = NEGATIVE WEIGHTS NOT PERMITTED
 MAXIT- MAX NO OF ITERATIONS       3Ø   ITERATIONS (MAX)
 EPSI  - CONVERGENCE CRITERION     Ø.ØØ1Ø = MINIMUM SSTRESS IMPROVEMENT

I/O OPTIONS-

 NDT   - PRINT DATA, DISTANCES AND DISPARITIES      1 = DO PRINT
 NPT   - PLOT RESULTS                               1 = DO PLOT
 NPH   - PUNCH RESULTS                              Ø = DO NOT PUNCH
INDATA- DATA INPUT UNIT NUMBER                      1 = DATA FROM CARDS
INITX  - INITIAL STIMULUS COORDINATES               Ø = COMPUTE
INITW  - INITIAL SUBJECT WEIGHTS                    Ø = COMPUTE
INITWS- INITIAL STIMULUS WEIGHTS                    Ø = COMPUTE
TOTAL MEMORY REQUIRED FOR THIS PROBLEM IS    5963 WORDS.
INPUT DATA FORMAT-
     (6F)
```

INPUT DATA MATRIX
SUBJECT 1

	1	2	3	4	5	6
1	0.000	0.300	0.001	0.058	0.001	0.117
2	0.190	0.000	0.001	0.058	0.001	0.034
3	0.001	0.015	0.000	0.001	0.001	0.001
4	0.333	0.136	0.001	0.000	0.001	0.206
5	0.001	0.045	0.500	0.500	0.000	0.241
6	0.001	0.015	0.001	0.001	0.166	0.000

SUBJECT 1 HAS 0 MISSING OBSERVATIONS.

***** WARNING INCONSISTENT CONTROL PARAMETERS
THE NUMBER OF PARAMETERS BEING COMPUTED (36)
MAY BE TOO LARGE FOR RELIABLE RESULTS

ITERATION HISTORY FOR THE 3 DIMENSIONAL SOLUTION
(IN SQUARED DISTANCES)

ITERATION	STRESS	IMPROVEMENT
1	0.26705	
2	0.16220	0.10486
3	0.13219	0.03001
4	0.11630	0.01589
5	0.10211	0.01420
6	0.09262	0.00949
7	0.08805	0.00457
8	0.08565	0.00239
9	0.08410	0.00155
10	0.08312	0.00098

STRESS AND PHI (IN DISTANCES)

STRESS = .129 PHI = .983

CONFIGURATION DERIVED IN 3 DIMENSIONS

STIMULUS COORDINATES	DIMENSION		
STIMULUS	1	2	3
1 (Sc)	0.1790	1.2240	-0.2586
2 (Cu)	-0.5507	1.2994	-1.2899
3 (Ac)	-1.9562	-0.8049	0.6022
4 (Ci)	0.6314	0.2359	1.2739
5 (Cs)	0.8617	-1.2933	0.8922
6 (Cb)	0.8348	-0.6611	-1.2197

STIMULUS WEIGHTS	DIMENSION		
STIMULUS	1	2	3
1	0.2906	0.2519	0.8653
2	1.6935	0.0000	0.0000
3	0.3905	0.3152	0.1418
4	0.2774	1.0306	0.0000
5	0.0000	0.3019	0.1907
6	0.2381	0.5795	0.4529

DISTANCES

SUBJECT 1

	1	2	3	4	5	6
1	0.000	1.038	1.733	1.529	1.696	1.349
2	0.950	0.000	1.829	1.538	1.838	1.803
3	1.784	1.635	0.000	1.738	1.785	1.876
4	1.031	1.246	1.724	0.000	1.557	0.917
5	1.472	1.714	0.297	0.857	0.000	0.986
6	1.606	1.639	1.836	1.814	1.501	0.000

DISPARITIES (OPTIMALLY SCALED DATA)

SUBJECT 1

	1	2	3	4	5	6
1	0.321	0.985	1.739	1.534	1.739	1.369
2	0.985	0.321	1.739	1.534	1.739	1.699
3	1.739	1.699	0.321	1.739	1.739	1.739
4	0.985	1.369	1.739	0.321	1.739	0.985
5	1.739	1.699	0.321	0.321	0.321	0.985
6	1.739	1.699	1.739	1.739	1.369	0.321

***** WARNING INCONSISTENT CONTROL PARAMETERS
THE NUMBER OF PARAMETERS BEING COMPUTED (24)
MAY BE TOO LARGE FOR RELIABLE RESULTS

ITERATION HISTORY FOR THE 2 DIMENSIONAL SOLUTION
(IN SQUARED DISTANCES)

ITERATION	STRESS	IMPROVEMENT
1	0.33595	
2	0.20626	0.12968
3	0.16908	0.03718
4	0.14825	0.02083
5	0.13132	0.01693
6	0.12472	0.00660
7	0.12306	0.00166
8	0.12247	0.00059

STRESS AND PHI (IN DISTANCES)

STRESS = .174 PHI = .970

CONFIGURATION DERIVED IN 2 DIMENSIONS

STIMULUS COORDINATES

STIMULUS	DIMENSION 1	DIMENSION 2
1	1.1775	-0.0604
2	1.1710	0.1351
3	-1.3885	0.4608
4	0.2992	1.7649
5	-1.0943	-1.2011
6	-0.1649	-1.0993

STIMULUS WEIGHTS

STIMULUS	DIMENSION 1	DIMENSION 2
1	0.4631	0.4410
2	0.4448	0.5558
3	0.4560	0.8373
4	1.1502	0.0479
5	0.5102	0.0000
6	1.5282	0.2687

DISTANCES

SUBJECT 1

	1	2	3	4	5	6
1	0.000	0.130	1.780	1.351	1.722	1.145
2	0.146	0.000	1.724	1.347	1.810	1.281
3	1.797	1.754	0.000	1.650	1.534	1.649
4	1.023	1.001	1.832	0.000	1.629	0.800
5	1.623	1.618	0.210	0.995	0.000	0.664
6	1.745	1.771	1.715	1.592	1.150	0.000

DISPARITIES (OPTIMALLY SCALED DATA)

SUBJECT 1

	1	2	3	4	5	6
1	0.360	0.658	1.710	1.349	1.710	1.101
2	0.658	0.360	1.710	1.349	1.710	1.459
3	1.710	1.710	0.360	1.710	1.710	1.710
4	0.658	1.101	1.710	0.360	1.710	0.658
5	1.710	1.459	0.360	0.360	0.360	0.658
6	1.710	1.710	1.710	1.710	1.101	0.360